Mathematical Models and Contact Simulations of Concave Beveloid Gears

Chia-Chang Liu
Assistant Professor,
Department of Mechanical Engineering,
Ching Yun Institute of Technology,
Jung-Li, Taiwan 320, R.O.C.

Chung-Biau Tsay
Professor, Mem. ASME,
Department of Mechanical Engineering,
National Chiao Tung University,
Hsinchu, Taiwan 30010, R.O.C.

This study presents two mathematical models of concave beveloid gears ground by Mitome's grinding method and by the novel grinding method proposed by the authors. Based on the developed mathematical models, the contact simulations are performed and the characteristics of concave beveloid gear pairs are investigated. Simulation results indicate that our novel grinding method ameliorates the drawback of Mitome's grinding method by eliminating the transmission error of the helical concave beveloid gear pairs. In contrast to conventional beveloid gear pairs, the gears ground by the proposed novel grinding method not only have larger contact ellipses, but also mesh conjugately with non-parallel axes, although assembly errors exist. [DOI: 10.1115/1.1517563]

1 Introduction

Beveloid gears, also known as conical involute gears, are involute gears with tapered tooth thicknesses, roots and outside diameters. Beveloid gears can transmit rotational motion between parallel, intersected and crossed axes in any relative position, and they are not sensitive to assembly errors under non-parallel axes meshing. However, beveloid gears remain relatively little studied, with Mitome [1–7] having conducted most of the research in this field. Mitome [1,3] performed and analyzed taper hobbing methods for beveloid gear generations. Mitome [2] studied theoretically and experimentally the tooth action of a beveloid gear pair. Mitome [4] also proposed a design for crossed axes beveloid gears and established their engagement models. Theoretically, the bearing contacts of beveloid gear pairs under non-parallel axes meshing are point contacts, and the contact ellipses are relatively small. The low-load capacity thus limits the application of gear pairs to power transmission. To improve the load capacity, Mitome et al. [5–7] proposed the idea of concave beveloid gears generated by the infeed grinding method. Although the grinding method proposed by Mitome can enlarge the contact ellipses of beveloid gear pairs, it is impractical for helical concave beveloid gear pairs, since transmission error (TE) is induced even under ideal assembly conditions. To overcome this problem, a novel grinding method for the manufacture of helical concave beveloid gear is proposed herein.

Although the previous studies have significantly improved understanding of the characteristics of beveloid gears, they did not establish a complete mathematical model and simulate the contact of concave beveloid gear pairs. This study develops mathematical models of concave beveloid gear pairs according to Mitome's grinding method and the novel grinding method proposed herein. Based on the developed mathematical models, investigations involving tooth contact analysis (TCA) and contact ellipse simulations are carried out. Results in this study not only verify the superiority of the novel grinding method proposed by the authors, but also reflect the contact nature of concave beveloid gear pairs.

2 Mathematical Models of Concave Beveloid Gear Pairs

2.1 Generation Concept. According to Mitome's research [5–7], the concave beveloid gears described below are manufactured based on the infeed grinding mechanism shown in Fig. 1. Figure 1(*a*) illustrates the infeed grinding mechanism for straight concave beveloid gears. A corresponding imaginary rack cutter which generates the conventional beveloid gear is presented here for reference. The pitch plane of the corresponding imaginary rack cutter is set to form a cone angle δ with respect to the gear axis of revolution. The pitch circle of the gear and the pitch plane of the corresponding imaginary rack cutter are in tangency at pitch point P_0, and r denotes the pitch radius of the gear. During grinding, the grinding wheel feeds along the infeed direction, which is perpendicular to the pitch plane of the corresponding imaginary rack cutter, and does not travel along the lengthwise direction of the gear tooth as in spur and helical gear grindings. Meanwhile, the gear rotates with angular velocity ω and the grinding wheel translates in the tangential direction of the gear pitch circle with velocity $r\omega$. Notably, the grinding wheel can be regarded as the imaginary rack cutter when its pitch radius r_w approaches infinity (i.e., $r_w=\infty$).

Figure 1(*b*) presents a view perpendicular to the pitch plane of the corresponding imaginary rack cutter, where the grinding wheel is assigned a helix angle β to satisfy the grinding requirements for helical concave beveloid gears. Referring to the grinding method of the helical concave beveloid gear proposed by Mitome et al. [7], although the grinding wheel is set with a helix angle β, it still translates with the same velocity $r\omega$ as in the grinding of straight concave beveloid gears. However, helical concave beveloid gear pairs ground by this method may induce transmission errors even under ideal assembly conditions. To overcome this predicament, a novel grinding method is proposed herein by translating the grinding wheel along its axial direction, which is perpendicular to the tooth trace direction, with velocity $r\omega\cos\beta$, as illustrated in Fig. 1(*b*). Therefore, the proposed novel grinding method can be termed as ''grinder-axial-translating grinding method.'' Notably, Mitome's grinding method and the novel grinding method are identical for the grinding of straight concave beveloid gears for which is $\beta=0$deg.

In this investigation, the beveloid gear pair used in the contact simulation comprises the pinion Σ_1 and the gear Σ_2, which are generated by grinding wheels Σ_F and Σ_G, respectively. Since the generation processes are identical, the subscripts $i=1$ and 2 represent the pinion Σ_1 and gear Σ_2, while $j=F$ and G represent their corresponding grinding wheels Σ_F and Σ_G, in the following derivation.

2.2 Mathematical Model of Grinding Wheel Σ_j. As illustrated in Fig. 2(*a*), the straight edge $\overline{M_0^{(j)}M_2^{(j)}}$ on the axial section of the grinding wheel can be represented in coordinate system

Contributed by the Power Transmission and Gearing Committee for publication in the JOURNAL OF MECHANICAL DESIGN. Manuscript received April 2001. Associate Editor: R. F. Handschah.

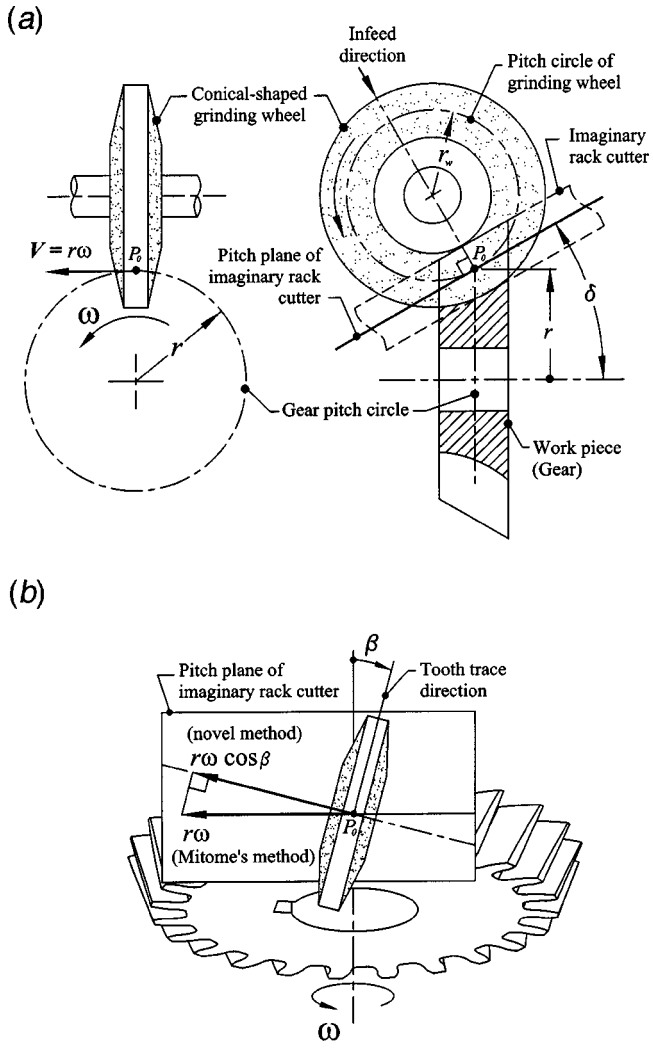

Fig. 1 Infeed grinding mechanism for concave beveloid gears

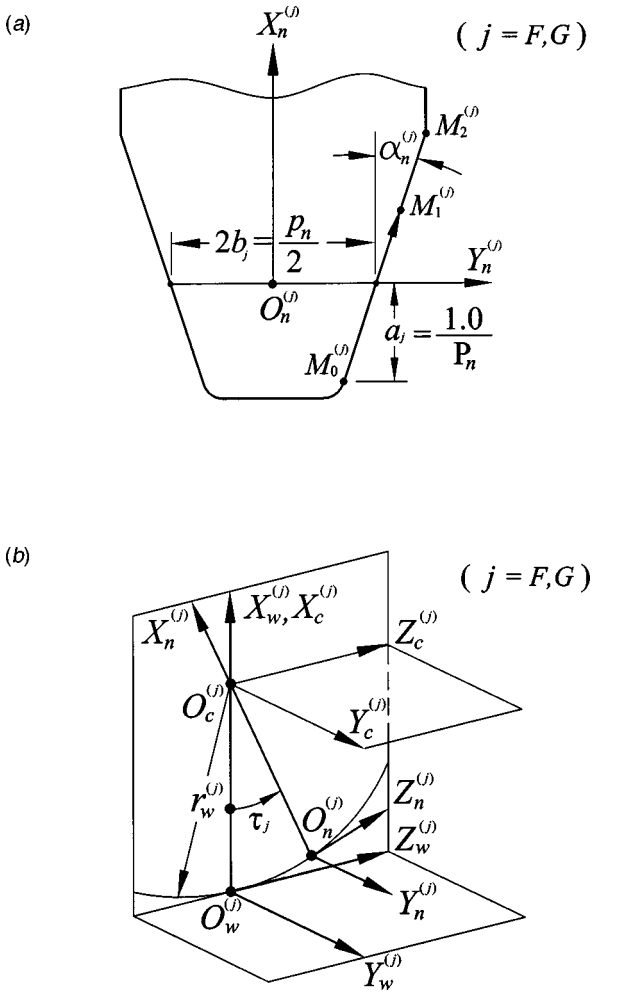

Fig. 2 Formation of the grinding wheel surface Σ_j in coordinate system $S_w^{(j)}(X_w^{(j)}, Y_w^{(j)}, Z_w^{(j)})$

$S_n^{(j)}(X_n^{(j)}, Y_n^{(j)}, Z_n^{(j)})$ by

$$x_n^{(j)} = \ell_j \cos\alpha_n^{(j)} - a_j,$$
$$y_n^{(j)} = \ell_j \sin a_n^{(j)} - a_j \tan\alpha_n^{(j)} + b_j,$$
$$\text{and} \quad z_n^{(j)} = 0, \tag{1}$$

where $\ell_j = |\overline{M_0^{(j)} M_1^{(j)}}|$ is a linear parameter, $\alpha_n^{(j)}$ denotes the normal pressure angle, and P_n and p_n represent the diametral pitch and circular pitch, respectively. The mathematical model of grinding wheel surface Σ_j can be established by considering the coordinate systems shown in Fig. 2(*b*). Let the above-mentioned axial section, which is attached to plane $X_n^{(j)} - Y_n^{(j)}$, rotate by an angle τ_j along a circular arc with radius $r_w^{(j)}$ and center at $O_c^{(j)}$, with respect to the $Y_c^{(j)}$-axis, the profile of grinding wheel Σ_j sweeps out the surface in coordinate system $S_w^{(j)}(X_w^{(j)}, Y_w^{(j)}, Z_w^{(j)})$ as follows:

$$\mathbf{R}_w^{(j)} = \begin{bmatrix} x_w^{(j)} \\ y_w^{(j)} \\ z_w^{(j)} \end{bmatrix} = \begin{bmatrix} \cos\tau_j(\ell_j \cos\alpha_n^{(j)} - a_j) + (r_w^{(j)} - r_w^{(j)} \cos\tau_j) \\ \ell_j \sin\alpha_n^{(j)} - a_j \tan\alpha_n^{(j)} + b_j \\ -\sin\tau_j(\ell_j \cos\alpha_n^{(j)} - a_j) + r_w^{(j)} \sin\tau_j \end{bmatrix}. \tag{2}$$

Herein, $r_w^{(j)}$ represents the pitch radius of the grinding wheel. Furthermore, the unit normal of the grinding wheel surface can be obtained in coordinate system $S_w^{(j)}$ by

$$\mathbf{n}_w^{(j)} = \begin{bmatrix} n_{xw}^{(j)} \\ n_{yw}^{(j)} \\ n_{zw}^{(j)} \end{bmatrix} = \begin{bmatrix} \sin\alpha_n^{(j)} \cos\tau_j \\ -\cos\alpha_n^{(j)} \\ -\sin\alpha_n^{(j)} \sin\tau_j \end{bmatrix}. \tag{3}$$

2.3 Gears Ground by Mitome's Grinding Method. Figure 3 displays the coordinate systems of the grinding wheel Σ_j and the generated gear Σ_i during the generation process. According to Fig. 3(*a*), the plane $Y_r^{(j)} - Z_r^{(j)}$ of coordinate system $S_r^{(j)}(X_r^{(j)}, Y_r^{(j)}, Z_r^{(j)})$, which represents the pitch plane of the corresponding imaginary rack cutter, is set to form an inclination angle δ_i with respect to the plane $Y_a^{(j)} - Z_a^{(j)}$, which represents the plane axode of the cylindrical gear. Herein, δ_i denotes the cone angle of the generated gear Σ_i; r_i represents the pitch radius and ϕ_i denotes the rotation angle of the generated gear. Coordinate system $S_b^{(j)}(X_b^{(j)}, Y_b^{(j)}, Z_b^{(j)})$ is the reference coordinate system, while coordinate system $S_i(X_i, Y_i, Z_i)$ is attached to the generated gear Σ_i. Figure 3(*b*) shows the position of the grinding wheel Σ_j on the pitch plane of the corresponding imaginary rack cutter, plane $Y_r^{(j)} - Z_r^{(j)}$, during grinding. Coordinate system $S_{w0}^{(j)}(X_{w0}^{(j)}, Y_{w0}^{(j)}, Z_{w0}^{(j)})$, which forms a helix angle β_i with respect to coordinate system $S_r^{(j)}$, can be regarded as the initial position of grinding wheel coordinate system $S_w^{(j)}$ when the generated gear rotation angle $\phi_i = 0$ deg. According to Mitome's grinding method, the origin of the grinding wheel coordinate system $S_w^{(j)}$ translates along the $Y_r^{(j)}$-axis during generation. Grinding

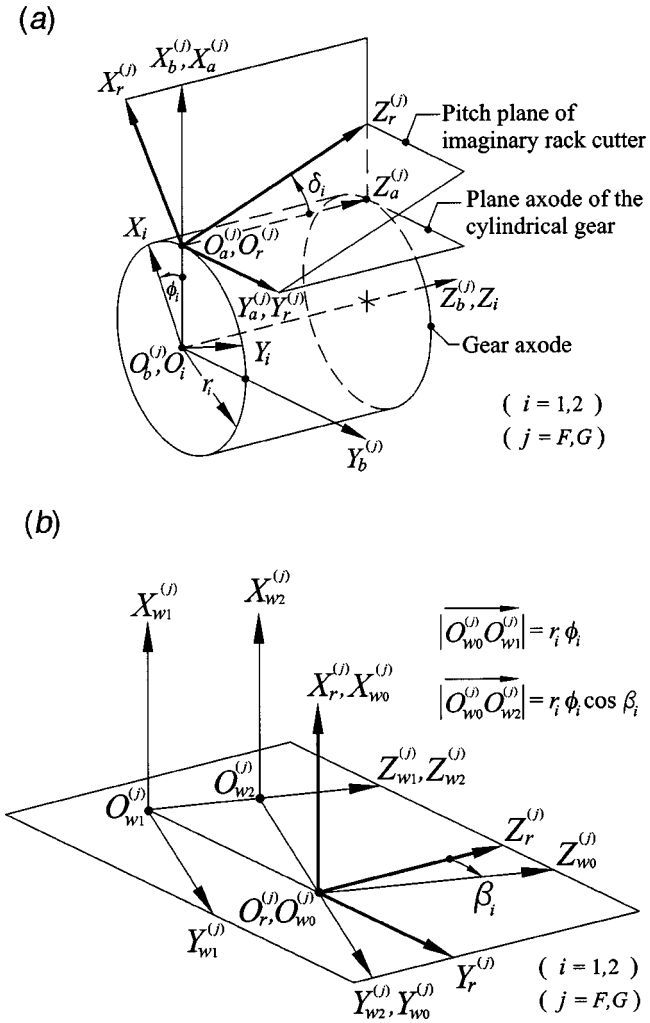

Fig. 3 Coordinate relationship between the grinding wheel and the generated gear

wheel coordinate system $S_w^{(j)}$ can thus be described by $S_{w1}^{(j)}(X_{w1}^{(j)}, Y_{w1}^{(j)}, Z_{w1}^{(j)})$ when gear Σ_i rotates through an angle ϕ_i, and $|O_{w0}^{(j)}O_{w1}^{(j)}| = r_i\phi_i$ is the translational displacement of the grinding wheel Σ_j. Based on the theory of gearing proposed by Litvin [8,9], the generated gear surface Σ_i can be obtained by simultaneously considering the locus of the grinding wheel surface Σ_j, represented in gear coordinate system S_i, together with the equation of meshing between the grinding wheel and the generated gear.

Let $\mathbf{R}_b^{(j)}$ and $\mathbf{n}_b^{(j)}$ respectively denote the position vector and unit normal of the grinding wheel surface Σ_j and generated gear surface Σ_i at their common contact point, represented in reference coordinate system $S_b^{(j)}$. According to the coordinate systems displayed in Fig. 3 and Eq. (3), $\mathbf{n}_b^{(j)}$ can be obtained by

$$\mathbf{n}_b^{(j)} = \begin{bmatrix} \cos\delta_i\, n_{xw}^{(j)} - \sin\delta_i \sin\beta_i\, n_{yw}^{(j)} + \sin\delta_i \cos\beta_i n_{zw}^{(j)} \\ \cos\beta_i n_{yw}^{(j)} + \sin\beta_i n_{zw}^{(j)} \\ -\sin\delta_i n_{xw}^{(j)} - \cos\delta_i \sin\beta_i n_{yw}^{(j)} + \cos\delta_i \cos\beta_i n_{zw}^{(j)} \end{bmatrix}. \quad (4)$$

The angular velocity of the generated gear Σ_i can be acquired in coordinate system $S_b^{(j)}$ by

$$\omega_b^{(i)} = \frac{d\phi_i}{dt} = \begin{bmatrix} 0 \\ 0 \\ -\omega_i \end{bmatrix}. \quad (5)$$

Furthermore, the velocities of the grinding wheel surface Σ_j and the generated gear surface Σ_i at their common contact point can be expressed by $\mathbf{V}_b^{(j)}$ and $\mathbf{V}_b^{(i)}$, respectively, as follows:

$$\mathbf{V}_b^{(j)} = \begin{bmatrix} 0 \\ -r_i\omega_i \\ 0 \end{bmatrix}, \quad (6)$$

and $\mathbf{V}_b^{(i)} = \omega_b^{(i)} \times \mathbf{R}_b^{(j)}$

$$= \omega_i \begin{bmatrix} \cos\beta_i y_w^{(j)} + \sin\beta_i z_w^{(j)} - r_i\phi_i \\ -\cos\delta_i x_w^{(j)} + \sin\delta_i \sin\beta_i y_w^{(j)} - \sin\delta_i \cos\beta_i z_w^{(j)} - r_i \\ 0 \end{bmatrix}. \quad (7)$$

The equation of meshing can be obtained by applying the orthogonality of the relative velocity and surface common normal of the grinding wheel surface Σ_j and the generated gear surface Σ_i. The following equation can thus be observed:

$$\mathbf{n}_b^{(j)} \cdot \mathbf{V}_b^{(ji)} = \mathbf{n}_b^{(j)} \cdot (\mathbf{V}_b^{(j)} - \mathbf{V}_b^{(i)}) = 0. \quad (8)$$

Substituting Eqs. (4), (6) and (7) into Eq. (8) enables us to obtain the equation of meshing for Mitome's grinding method. According to Fig. 3, the locus of the grinding wheel represented in coordinate system S_i can be obtained as follows:

$$\begin{aligned} x_i &= (\cos\phi_i \cos\delta_i) x_w^{(j)} - (\sin\phi_i \cos\beta_i + \cos\phi_i \sin\delta_i \sin\beta_i) y_w^{(j)} \\ &\quad - (\sin\phi_i \sin\beta_i - \cos\phi_i \sin\delta_i \cos\beta_i) z_w^{(j)} + A_i, \\ y_i &= (\sin\phi_i \cos\delta_i) x_w^{(j)} + (\cos\phi_i \cos\beta_i - \sin\phi_i \sin\delta_i \sin\beta_i) y_w^{(j)} \\ &\quad + (\cos\phi_i \sin\beta_i + \sin\phi_i \sin\delta_i \cos\beta_i) z_w^{(j)} + B_i, \\ \text{and} \quad z_i &= -\sin\delta_i x_w^{(j)} - \cos\delta_i \sin\beta_i y_w^{(j)} + \cos\delta_i \cos\beta_i z_w^{(j)} + C_i. \end{aligned} \quad (9)$$

where

$$A_i = r_i\phi_i \sin\phi_i + r_i \cos\phi_i, \quad (10)$$

$$B_i = -r_i\phi_i \cos\phi_i + r_i \sin\phi_i, \quad (11)$$

$$\text{and} \quad C_i = 0. \quad (12)$$

Hence, the tooth surface of the generated gear Σ_i ground by Mitome's grinding method can be expressed by Eqs. (8) and (9). The unit normal vector of the generated tooth surface can be attained by

$$\begin{aligned} n_{xi} &= (\cos\phi_i \cos\delta_i) n_{xw}^{(j)} - (\sin\phi_i \cos\beta_i + \cos\phi_i \sin\delta_i \sin\beta_i) n_{yw}^{(j)} \\ &\quad - (\sin\phi_i \sin\beta_i - \cos\phi_i \sin\delta_i \cos\beta_i) n_{zw}^{(j)}, \\ n_{yi} &= (\sin\phi_i \cos\delta_i) n_{xw}^{(j)} + (\cos\phi_i \cos\beta_i - \sin\phi_i \sin\delta_i \sin\beta_i) n_{yw}^{(j)} \\ &\quad + (\cos\phi_i \sin\beta_i + \sin\phi_i \sin\delta_i \cos\beta_i) n_{zw}^{(j)}, \\ \text{and} \quad n_{zi} &= -\sin\delta_i n_{xw}^{(j)} - \cos\delta_i \sin\beta_i n_{yw}^{(j)} + \cos\delta_i \cos\beta_i n_{zw}^{(j)}. \end{aligned} \quad (13)$$

2.4 Gears Ground by the Novel Grinding Method. In the novel grinding process proposed herein, the grinding wheel Σ_j translates along the direction of its axis of revolution as presented in Fig. 1(*b*). Therefore, the origin of the grinding wheel coordinate system $S_w^{(j)}$ translates along the $Y_{w0}^{(j)}$-axis instead of the $Y_r^{(j)}$-axis during generation, as shown in Fig. 3(*b*). The position of the grinding wheel coordinate system $S_w^{(j)}$ can be represented by $S_{w2}^{(j)}(X_{w2}^{(j)}, Y_{w2}^{(j)}, Z_{w2}^{(j)})$ when the generated gear Σ_i rotates through an angle ϕ_i, and the translational distance of the grinding wheel is $|\overline{O_{w0}^{(j)}O_{w2}^{(j)}}| = r_i\phi_i \cos\beta_i$. Notably, the unit normal vector of the

grinding wheel $\mathbf{n}_b^{(j)}$ is the same as in Eq. (4), but the velocities of the grinding wheel Σ_j and the generated gear Σ_i at their point of contact now become

$$\mathbf{V}_b^{(j)} = r_i \omega_i \begin{bmatrix} \sin\delta_i \sin\beta_i \cos\beta_i \\ -\cos^2\beta_i \\ \cos\delta_i \sin\beta_i \cos\beta_i \end{bmatrix}, \tag{14}$$

and

$$\mathbf{V}_b^{(i)} = \omega_b^{(i)} \times \mathbf{R}_b^{(j)} = \omega_i \begin{bmatrix} \cos\beta_i y_w^{(j)} + \sin\beta_i z_w^{(j)} - r_i \phi_i \cos^2\beta_i \\ (-\cos\delta_i x_w^{(j)} + \sin\delta_i \sin\beta_i y_w^{(j)} - \sin\delta_i \cos\beta_i z_w^{(j)} \\ -r_i \phi_i \sin\delta_i \sin\beta_i \cos\beta_i - r_i) \\ 0 \end{bmatrix}. \tag{15}$$

Substituting Eqs. (4), (14) and (15) into Eq. (8) allows us to solve the equation of meshing for proposed gears with this novel grinding method. Similarly, the tooth surface and unit normal vector of the gear Σ_i ground by the novel grinding method can be expressed by Eqs. (8)–(13) with the modification of Eqs. (10)–(12) as

$$A_i = r_i \phi_i (\sin\phi_i \cos\beta_i + \cos\phi_i \sin\delta_i \sin\beta_i) \cos\beta_i + r_i \cos\phi_i, \tag{16}$$

$$B_i = r_i \phi_i (-\cos\phi_i \cos\beta_i + \sin\phi_i \sin\delta_i \sin\beta_i) \cos\beta_i + r_i \sin\phi_i, \tag{17}$$

$$\text{and} \quad C_i = r_i \phi_i \cos\delta_i \sin\beta_i \cos\beta_i. \tag{18}$$

3 Meshing Model and Tooth Contact Analysis

Adopting the gear engagement concept proposed by Mitome [4], Fig. 4 illustrates the schematic meshing model of the beveloid gear pair. The beveloid pinion Σ_1 and gear Σ_2 can be considered to be two imaginary cones with cone angles δ_1 and δ_2, lying on opposite sides of the pitch plane of the imaginary engaging rack, while $S_f(X_f, Y_f, Z_f)$ and $S_g(X_g, Y_g, Z_g)$ are the reference coordinate systems for the pinion coordinate system $S_1(X_1, Y_1, Z_1)$ and gear coordinate system $S_2(X_2, Y_2, Z_2)$, respectively. Furthermore, ϕ_1' and ϕ_2' denote the rotation angles of the pinion and gear during meshing. Points O_f and O_g are the centers of the pitch circles

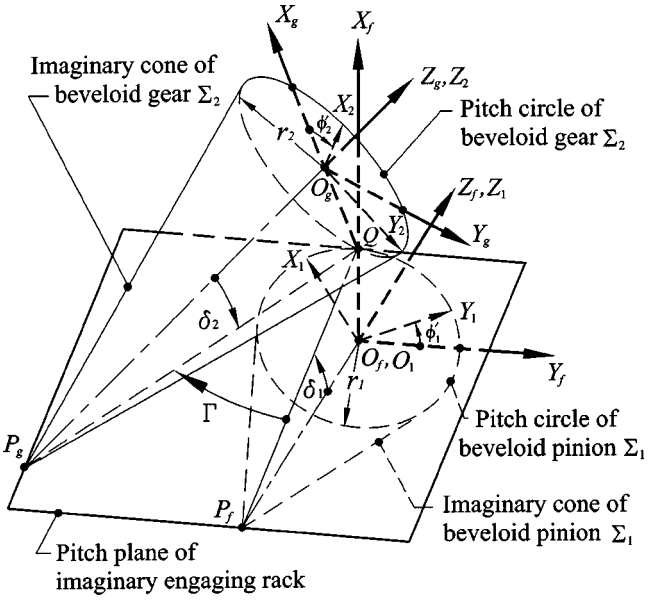

Fig. 4 Schematic relationship for the meshing of pinion, gear and the pitch plane of the imaginary engaging rack

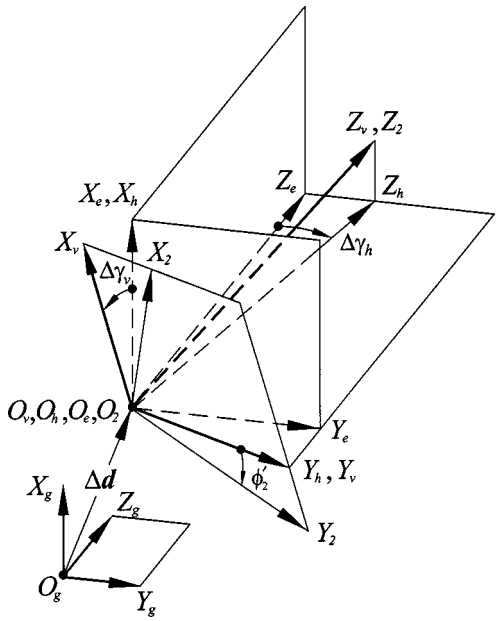

Fig. 5 Assembly error simulation of the beveloid gear

of the pinion and gear, where r_1 and r_2 denote their respective pitch radii, and P_f and P_g are the apexes of the imaginary cones. The pitch circles of the pinion Σ_1 and gear Σ_2 are tangent to the pitch plane at point Q, and the tangent lines of the two imaginary cones with respect to the pitch plane of the imaginary engaging rack, $\overline{P_f Q}$ and $\overline{P_g Q}$, form an angle $\Gamma = \beta_1 + \beta_2$. To investigate the meshing of a beveloid gear pair with assembly errors, auxiliary coordinate systems $S_e(X_e, Y_e, Z_e)$, $S_h(X_h, Y_h, Z_h)$ and $S_v(X_v, Y_v, Z_v)$ have been set up as displayed in Fig. 5. Coordinate system S_e is set up and its orientation in respect to coordinate system S_g is maintained. The offset $\overline{O_g O_e} = \Delta\mathbf{d} = (\Delta x_g, \Delta y_g, \Delta z_g)$ indicates the mounting position deviation of the gear with respect to its ideal assembly position. Moreover, coordinate system S_h simulates the gear with a horizontal angular misalignment $\Delta\gamma_h$ with respect to coordinate system S_e, while coordinate system S_v simulates the gear with a vertical angular misalignment $\Delta\gamma_v$ with respect to coordinate system S_h. Coordinate system S_v thus simulates the gear with assembly errors $\Delta\mathbf{d}$, $\Delta\gamma_h$ and $\Delta\gamma_v$.

Applying the coordinate transformation matrix equation, the position vectors and unit normal vectors of the pinion and gear surfaces can be represented in coordinate system S_f. The mating pinion and gear tooth surfaces must satisfy the following conditions at their instantaneous contact point [8,9]:

$$\mathbf{R}_f^{(1)} = \mathbf{R}_f^{(2)}, \tag{19}$$

$$\text{and} \quad \mathbf{n}_f^{(1)} = \pm \mathbf{n}_f^{(2)}, \tag{20}$$

where $\mathbf{R}_f^{(1)}$ and $\mathbf{R}_f^{(2)}$ are the position vectors while $\mathbf{n}_f^{(1)}$ and $\mathbf{n}_f^{(2)}$ denote the unit normal vectors of pinion Σ_1 and gear Σ_2, represented in coordinate system S_f, respectively. In a three-dimensional space, Eqs. (19) and (20) form a system of five independent nonlinear equations with six unknowns: ϕ_1', ℓ_F, τ_F, ϕ_2', ℓ_G and τ_G. By choosing the pinion rotation angle ϕ_1' as an input variable, all other unknowns can be solved in terms of ϕ_1'. The instantaneous contact points on the pinion and gear surfaces can be obtained by substituting the solved unknowns into the pinion and gear tooth-surface equations. The deviation of the real gear rotation angle $\phi_2'(\phi_1')$ from its ideal rotation angle is defined as the transmission error (TE) which can be expressed as follows:

$$\mathrm{TE}=(\phi_2'-\phi_2'^{(0)})-\frac{T_1}{T_2}(\phi_1'-\phi_1'^{(0)}), \tag{21}$$

where $\phi_1'^{(0)}$ and $\phi_2'^{(0)}$ represent the initial values of ϕ_1' and ϕ_2', while T_1 and T_2 denote the tooth numbers of the pinion and gear, respectively.

4 Contact Ellipses

Theoretically, the bearing contact of a beveloid gear pair under non-parallel axes meshing is a point contact. Owing to the elasticity of tooth surface, the contact is spread over an elliptical area centered at the instantaneous contact point, which can be determined from the TCA result. Applying the methodologies developed by Litvin [8,9], the principal directions and curvatures of the pinion and gear tooth surfaces can be derived in terms of their corresponding cutting tool surfaces. Let $\mathbf{i}_I^{(i)}$ and $\mathbf{i}_{II}^{(i)}$ $(i=1,2)$ denote the principal directions of the pinion tooth surface Σ_1 and the gear tooth surface Σ_2 at their instantaneous contact point expressed in coordinate system S_f. At any instantaneous contact point, $\mathbf{i}_I^{(i)}$ and $\mathbf{i}_{II}^{(i)}$ $(i=1,2)$ are located on the common tangent plane of the mating pinion and gear tooth surfaces. The orientation of the contact ellipse with respect to $\mathbf{i}_I^{(1)}$ can be determined by angle η, as follows [8,9]:

$$\tan 2\eta=\frac{g_2\sin 2\sigma}{g_1-g_2\cos 2\sigma}, \tag{22}$$

$$\text{where}\quad g_i=\kappa_I^{(i)}-\kappa_{II}^{(i)}\quad (i=1,2). \tag{23}$$

Herein, $\kappa_{\mathrm{I}}^{(i)}$ and $\kappa_{\mathrm{II}}^{(i)}$ $(i=1,2)$ are the first and second principal curvatures of the mating pinion and gear tooth surfaces at contact point, and σ denotes the angle formed by $\mathbf{i}_I^{(1)}$ and $\mathbf{i}_I^{(2)}$. Meanwhile, the half length of the major and minor axes of the contact ellipse, a and b, can be expressed in terms of the elastic approach Δ by

$$a=\left|\frac{\Delta}{A}\right|^{1/2}, \tag{24}$$

$$\text{and}\quad b=\left|\frac{\Delta}{B}\right|^{1/2}, \tag{25}$$

where

$$A=\frac{1}{4}[\kappa_\Sigma^{(1)}-\kappa_\Sigma^{(2)}-(g_1^2-2g_1g_2\cos 2\sigma+g_2^2)^{1/2}], \tag{26}$$

$$B=\frac{1}{4}[\kappa_\Sigma^{(1)}-\kappa_\Sigma^{(2)}+(g_1^2-2g_1g_2\cos 2\sigma+g_2^2)^{1/2}], \tag{27}$$

$$\text{and}\quad \kappa_\Sigma^{(i)}=\kappa_I^{(i)}+\kappa_{II}^{(i)}\quad (i=1,2). \tag{28}$$

The elastic approach Δ for the contact ellipse simulation is selected herein as 0.00635 mm (0.00025 in), identical to the thickness of the coating paint used for contact pattern tests.

5 Numerical Illustrative Examples for Gear Contact Simulations

Figure 6 illustrates two typical types of gear mounting for concave beveloid gear pairs with intersected and crossed axes. Applying the computer simulation programs developed herein allow the TCA results to be obtained and contact ellipses to be plotted on the tooth surfaces. Table 1 lists some major design parameters of the beveloid gear pairs employed in the following examples. Notably, the same grinding wheel with pitch radius $r_w^{(j)}$ $(j=F,G)$ performed the gear tooth grinding for both pinion Σ_1 and gear Σ_2 in each case.

Example 1: Straight Concave Beveloid Gear Pair Mounted With Intersected Axes. As shown in Fig. 6(*a*), the gear pair in this example is composed of straight concave beveloid pinion and gear (i.e. $\beta_1=\beta_2=0$ deg) with cone angles $\delta_1=\delta_2=30$ deg, mounted with an intersection angle of 60 deg. Various grinding wheel pitch radii $r_w^{(j)}$ are selected to investigate the bearing contacts of the gear pair under ideal assembly conditions.

Case 1: $r_w^{(j)}=\infty$ (i.e. straight conventional beveloid gear).

Case 2: $r_w^{(j)}=50$ mm.

Case 3: $r_w^{(j)}=45$ mm.

According to Fig. 2, the intersection of the grinding wheel with the $X_w^{(j)}-Y_w^{(j)}$ plane (i.e. $\tau_j=0$) remains unchanged when $r_w^{(j)}$ varies. Therefore, by choosing $\tau_j=0$ in the mathematical model of tooth surfaces, the so-called line of coincidence can be acquired on the central region of the generated tooth surface Σ_i. The tooth surfaces are identical only on the line of coincidence with the variation of $r_w^{(j)}$, even when $r_w^{(j)}=\infty$, which makes the concave beveloid gear pair to the conventional beveloid gear pair. Table 2 summarizes the TCA results, and Fig. 7 illustrates the path of contact and the corresponding contact ellipses on the pinion tooth surface. According to the simulation results of Case 1, the straight conventional beveloid gear pair (i.e. $r_w^{(j)}=\infty$) meshes with TE $=0$, and the path of contact is identical with the line of coinci-

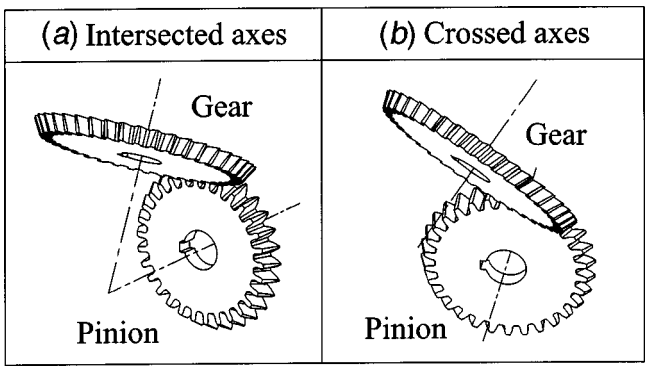

Fig. 6 Beveloid gear pairs with intersected and crossed axes

Table 1 Major design parameters of the beveloid pinion and gear

	Pinion Σ_1	Gear Σ_2
Number of teeth	$T_1=30$	$T_2=40$
Normal pressure angle	$\alpha_n^{(F)}=20°$	$\alpha_n^{(G)}=20°$
Normal module	$m_n=5\ (mm/teeth)$	

Table 2 TCA results of straight concave beveloid gear pair

CASE	ϕ_1' (deg.)	ℓ_F (mm)	τ_F (rad.)	ϕ_2' (deg.)	ℓ_G (mm)	τ_G (rad.)	TE(arc-sec.)
1	9.0	8.007	0.000	182.250	2.635	0.000	0.000
	6.0	6.664	0.000	180.000	3.978	0.000	0.000
2	3.0	5.321	0.000	177.750	5.321	0.000	0.000
3	0.0	3.978	0.000	175.500	6.664	0.000	0.000
	-3.0	2.635	0.000	173.250	8.007	0.000	0.000
4	9.0	8.269	-0.040	182.340	2.640	-0.042	0.000
	6.0	6.926	-0.040	180.090	3.983	-0.042	0.000
	3.0	5.583	-0.040	177.840	5.326	-0.042	0.000
	0.0	4.239	-0.040	175.590	6.669	-0.042	0.000
	-3.0	2.896	-0.040	173.340	8.012	-0.042	0.000
5	9.0	8.164	0.019	182.372	2.663	0.023	0.000
	6.0	6.821	0.019	180.122	4.006	0.023	0.000
	3.0	5.478	0.019	177.872	5.349	0.023	0.000
	0.0	4.135	0.019	175.622	6.692	0.023	0.000
	-3.0	2.792	0.019	173.372	8.036	0.023	0.000

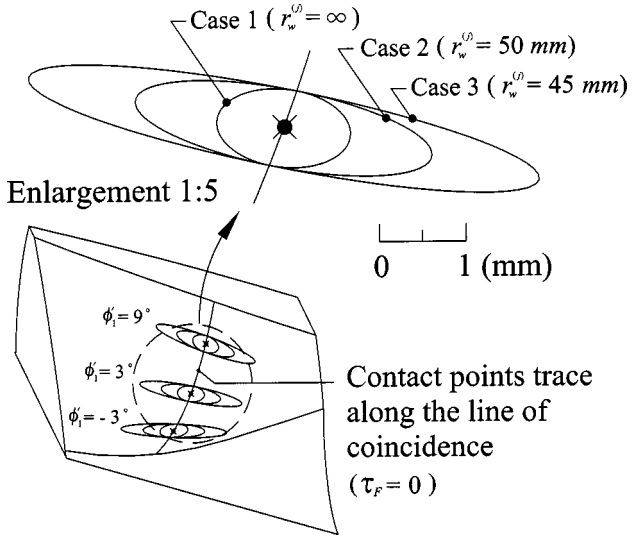

Fig. 7 Bearing contacts of the straight concave beveloid gear pair ground by grinding wheels with different $r_w^{(j)}$

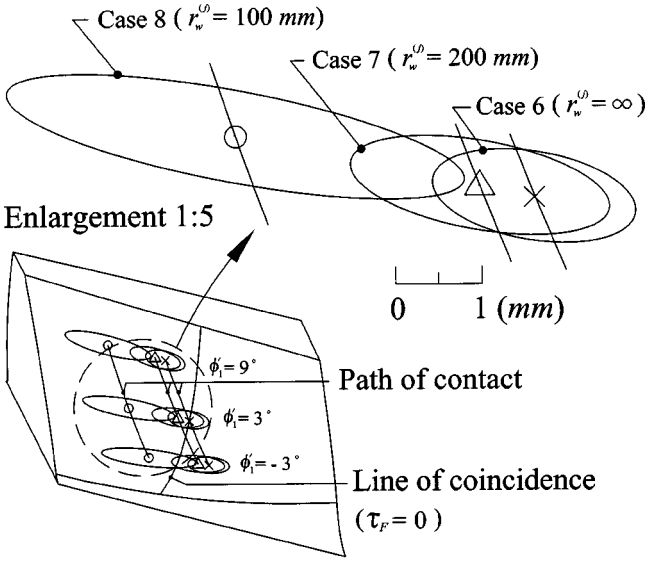

Fig. 9 Bearing contacts of helical concave beveloid gear pairs ground by Mitome's grinding method with different $r_w^{(j)}$

dence (i.e. $\tau_j = 0$). Since the tooth profile remains the same along the line of coincidence when the $r_w^{(j)}$ changes, it is reasonable to find that the straight concave beveloid gear pairs ground by grinding wheels with various $r_w^{(j)}$ still mesh with TE = 0, with their contact points tracing along the line of coincidence. Meanwhile, because a smaller pitch radius $r_w^{(j)}$ of the grinding wheel induces a larger bulgy deviation on the tooth surface except the line of coincidence, the contact ellipses enlarge significantly.

The gear pair ground by the grinding wheel with an appropriate pitch radius, $r_w^{(j)} = 50$ mm, is then chosen to simulate the contact of straight concave beveloid gear pairs with intersected axes under the following assembly conditions:

Case 4: $\Delta\gamma_h = \Delta\gamma_v = 0$ deg and $\Delta x_g = \Delta y_g = \Delta z_g = 0.3$ mm.

Case 5: $\Delta\gamma_h = 0.5$ deg, $\Delta\gamma_v = -0.2$ deg and $\Delta x_g = \Delta y_g = \Delta z_g = 0.3$ mm.

According to Table 2 and Fig. 8, even meshing under assembly errors, the TEs of the gear pair remain zero and the path of contact remains in the central region of the tooth surface. Therefore, the straight concave beveloid gear pairs mounted with intersected axes are insensitive to small assembly errors.

Example 2: Helical Concave Beveloid Gear Pair (Ground by Mitome's Grinding Method) Mounted With Crossed Axes In this example, the helical concave beveloid gear pair mounted with crossed axes, as illustrated in Fig. 6(*b*), is ground by Mitome's grinding method with $\delta_1 = \delta_2 = 20$ deg and $\beta_1 = \beta_2 = 15$ deg (right handed). Applying the algorithms proposed by Mitome [4], the shortest axial distance between two axes is 111.731 mm, while the crossed angle is calculated as 49.628 deg. The contact simulations of this helical concave beveloid gear pairs with crossed axes under ideal assembly conditions are performed using different grinding wheel pitch radii $r_w^{(j)}$ in the following cases.

Case 6: $r_w^{(j)} = \infty$ (i.e. helical conventional beveloid gear).

Case 7: $r_w^{(j)} = 200$ mm.

Case 8: $r_w^{(j)} = 100$ mm.

Figure 9 illustrates the bearing contacts of the gear pair plotted on the pinion tooth surface while Fig. 10 shows the TEs. According to the simulation results of Case 6, the helical conventional beveloid gear pair meshes conjugately and the TEs equal zero. However, the paths of contact are not identical with the line of

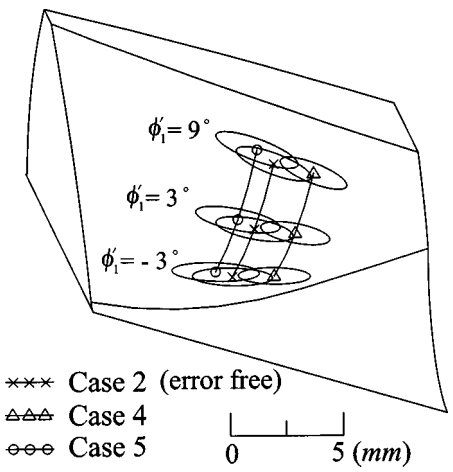

Fig. 8 Bearing contacts of the straight concave beveloid pair with assembly errors.

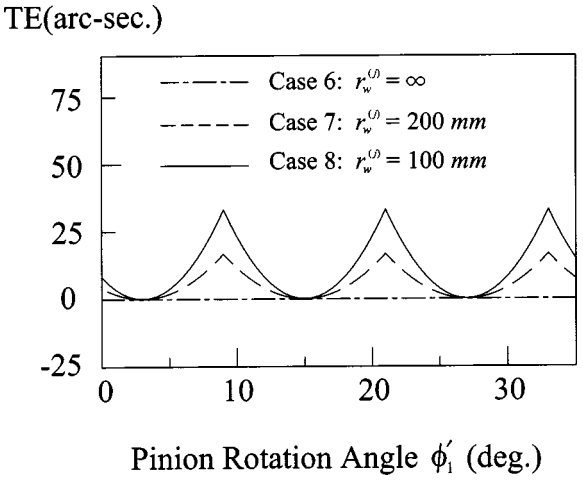

Fig. 10 Transmission errors of helical concave beveloid gear pairs ground by Mitome's grinding method

Table 3 TCA results of helical concave beveloid gear pairs ground by novel grinding method

CASE	ϕ_1' (deg.)	ℓ_F (mm)	τ_F (rad.)	ϕ_2' (deg.)	ℓ_G (mm)	τ_G (rad.)	TE(arc-sec.)
9 10 11	9.0	8.007	0.000	182.250	2.635	0.000	0.000
	6.0	6.664	0.000	180.000	3.978	0.000	0.000
	3.0	5.321	0.000	177.750	5.321	0.000	0.000
	0.0	3.978	0.000	175.500	6.664	0.000	0.000
	-3.0	2.635	0.000	173.250	8.007	0.000	0.000
12	9.0	8.283	-0.023	182.365	2.713	-0.023	0.000
	6.0	6.939	-0.023	180.115	4.057	-0.023	0.000
	3.0	5.596	-0.023	177.865	5.400	-0.023	0.000
	0.0	4.253	-0.023	175.615	6.743	-0.023	0.000
	-3.0	2.910	-0.023	173.365	8.086	-0.023	0.000
13	9.0	8.188	0.013	182.338	2.690	0.016	0.000
	6.0	6.845	0.013	180.088	4.033	0.016	0.000
	3.0	5.502	0.013	177.838	5.376	0.016	0.000
	0.0	4.159	0.013	175.588	6.719	0.016	0.000
	-3.0	2.816	0.013	173.338	8.062	0.016	0.000

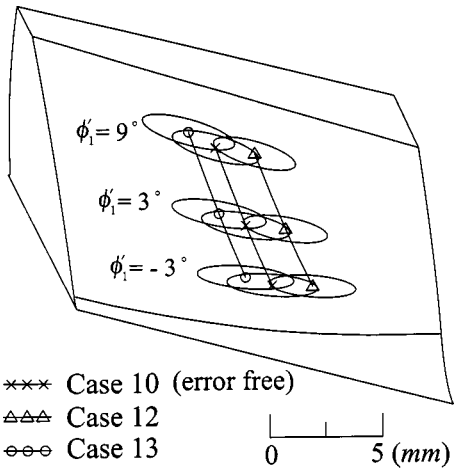

Fig. 12 Bearing contacts of helical concave beveloid pairs ground by novel grinding method with assembly errors

coincidence ($\tau_j = 0$) on the tooth surface ground by Mitome's grinding method. When the grinding wheel's pitch radius $r_w^{(j)}$ decreases from ∞ to 100 mm (Case 6 to Case 8), the bulgy deviation of the tooth surface, except for along the line of coincidence, results in the enlargement of the contact ellipses. However, the TEs increase and the characteristic of TE = 0 originally belonging to the helical conventional beveloid gear pair (i.e. $r_w^{(j)} = \infty$) is spoiled. Consequently, in the range of the considered design parameters, Mitome's grinding method is impractical for manufacturing an efficient helical concave beveloid gear pair with crossed axes.

Example 3: Helical Concave Beveloid Gear Pair (Ground by the Novel Grinding Method) Mounted With Crossed Axes The gear pair mentioned in Example 2 is now ground using the novel grinding method proposed in section 2.4. Cases 9 to 11 simulate the contact of the gear pair under ideal assembly conditions, with different pitch radii $r_w^{(j)}$ of the grinding wheel.

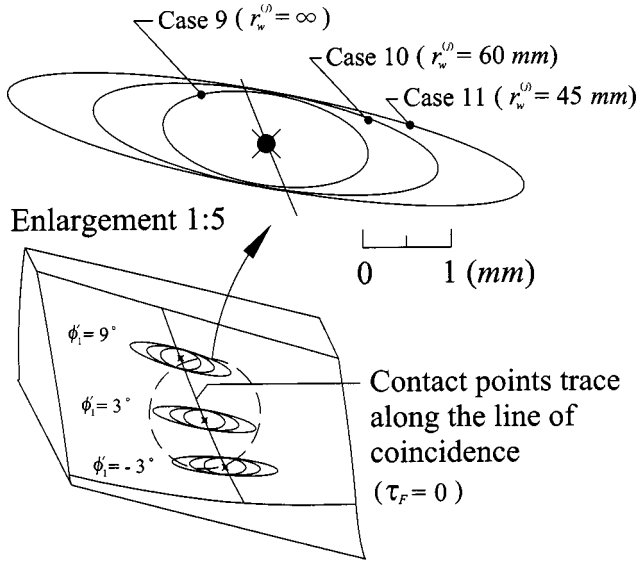

Fig. 11 Bearing contacts of helical concave beveloid gear pairs ground by novel grinding method with different $r_w^{(j)}$

Case 9: $r_w^{(j)} = \infty$ (i.e. helical conventional beveloid gear).
Case 10: $r_w^{(j)} = 60$ mm.
Case 11: $r_w^{(j)} = 45$ mm.

According to the TCA results listed in Table 3 and the bearing contacts illustrated in Fig. 11, the helical concave beveloid gear pair ground by the proposed novel grinding method can mesh with TE = 0 under the ideal assembly condition, and the path of contact is identical with the line of coincidence (i.e. $\tau_j = 0$). Meanwhile, the contact ellipses enlarge significantly as $r_w^{(j)}$ decreases. Hence, the novel grinding method ameliorates the defect of Mitome's grinding method in the grinding of helical concave beveloid gear pairs. The gear pair ground by the grinding wheel with an appropriate pitch radius, $r_w^{(j)} = 60$ mm, is then chosen to test the sensitivity of this gear pair to assembly errors as follows:
Case 12: $\Delta\gamma_h = \Delta\gamma_v = 0$ deg and $\Delta x_g = \Delta y_g = \Delta z_g = 0.3$ mm.
Case 13: $\Delta\gamma_h = 0.5$ deg, $\Delta\gamma_v = -0.2$ deg and $\Delta x_g = \Delta y_g = \Delta z_g = 0.3$ mm.

According to Table 3 and Fig. 12, even under assembly errors, the TEs of the gear pair remain zero and the path of contact remains in the central region of the tooth surface. These simulation results indicate that the helical concave beveloid gear pairs ground by the novel grinding method are insensitive to small assembly errors. The novel grinding method can also increase the load capacity of crossed axes helical gear pairs, which can be considered to be helical beveloid gear pairs with zero cone angles.

6 Conclusions

Simulation results in this study demonstrate that the novel grinding method proposed herein eliminates the transmission errors of helical beveloid gear pairs ground by Mitome's grinding method. Compared with conventional beveloid gear pairs, concave beveloid gear pairs not only solve the problems associated with low-load capacity by enlarging the contact ellipses, but also retain the special property of insensitivity to assembly errors under non-parallel axes meshing. The concave beveloid gear pairs thus fit the requirements of high load and highly precise motion transmission between non-parallel axes.

Acknowledgment

The authors are grateful to the National Science Council of the R.O.C. for the grant. Part of this work was performed under contract No. NSC 89-2212-E-009-084.

Nomenclature

a_F, a_G = design parameters of grinding wheels Σ_F and Σ_G (mm)
a = half-length of the major axis of the contact ellipse (mm)
b_F, b_G = design parameters of grinding wheels Σ_F and Σ_G (mm)
b = half-length of the minor axis of the contact ellipse (mm)
ℓ_F, ℓ_G = design parameters of grinding wheels Σ_F and Σ_G (mm)
P_n = gear diametral pitch (1/mm)
p_n = gear circular pitch (mm)
r_1, r_2 = pitch radii of the pinion Σ_1 and gear Σ_2 (mm)
$r_w^{(F)}$, $r_w^{(G)}$ = pitch radii of the grinding wheels Σ_F and Σ_G (mm)
T_1, T_2 = tooth numbers of the pinion Σ_1 and gear Σ_2
$\alpha_n^{(F)}$, $\alpha_n^{(G)}$ = normal pressure angles of grinding wheels Σ_F and Σ_G (degrees)
β_1, β_2 = helix angles on the pitch planes of the corresponding imaginary rack cutters of the pinion Σ_1 and gear Σ_2 (degrees)
δ_1, δ_2 = cone angles of pinion Σ_1 and gear Σ_2 (degrees)
ϕ_1, ϕ_2 = rotation angles of the pinion Σ_1 and gear Σ_2 in generating process (degrees)
ϕ_1', ϕ_2' = rotation angles of the pinion Σ_1 and gear Σ_2 during meshing (degrees)
$\phi_1'^{(0)}$, $\phi_2'^{(0)}$ = initial values of ϕ_1' and ϕ_2' during meshing (degrees)
τ_F, τ_G = design parameters of grinding wheels Σ_F and Σ_G (rad.)
Δ = elastic approach for the contact ellipse simulation (mm)
$\Delta\mathbf{d}$ = mounting position deviation of the gear with respect to its ideal assembly position (mm)
$\Delta\gamma_h$ = horizontal angular misalignment of the gear (degrees)
$\Delta\gamma_v$ = vertical angular misalignment of the gear (degrees)

References

[1] Mitome, K., 1981, "Table Sliding Taper Hobbing of Conical Gear Using Cylindrical Hob, Part 1: Theoretical Analysis of Table Sliding Taper Hobbing," ASME J. Ind., **103**, pp. 446–451.
[2] Mitome, K., 1985, "Conical Involute Gear, Part 3: Tooth Action of a Pair of Gears," Bull. JSME, **28**(245), pp. 2757–2764.
[3] Mitome, K., 1986, "Inclining Work-Arbor Taper Hobbing of Conical Gear Using Cylindrical Hob," ASME J. Mech. Des., **108**, pp. 135–141.
[4] Mitome, K., 1991, "Conical Involute Gear (Design of Nonintersecting-Nonparallel-Axis Conical Involute Gear)," JSME Int. J., Ser. III, **34**(2), pp. 265–270.
[5] Mitome, K., 1993, "Infeed Grinding of Straight Conical Involute Gear," JSME International Journal, Series C , **36**(4), pp. 537–542.
[6] Mitome, K., Ohmachi, T., Komatsubara, H., and Tamura, T., 1999, "Generating of Straight Concave Conical Gear," *Proceedings, 4th World Cong. on Gearing Power Transmission*, Paris, pp. 851-858.
[7] Komatsubara, H., Mitome, K., Ohmachi, T., and Watanabe, H., 1999, "Development of Concave Conical Gear Used for Marine Transmission," *Proceedings, 4th World Cong. on Gearing Power Transmission*, Paris, pp. 683-695.
[8] Litvin, F. L., 1989, *Theory of Gearing*, NASA Publication RP-1212, Washington D.C.
[9] Litvin, F. L., 1994, *Gear Geometry and Applied Theory*, Prentice Hall, New Jersey.